Gaussian curvature is represented with color. The low curvatures depicted in red correspond to less curved regions of the Fermi surface and are in accordance with the high-intensity points calculated for the charge variation in the vacuum. Diagonally opposite of the high intensities, we get only small oscillations resulting from the stronger curved regions shown in Fig. 3C. This result explains the triangular shape with a three fold symmetry instead of the six fold symmetry of the face-centered cubic-(111) surface.

Knowing the cone angle β of the focusing beams (Fig. 3A; β~60°) and the depth Z_{imp} of the impurity allows us to evaluate the diameter D of the LDOS pattern and vice versa. This result allows us to experimentally determine the position of impurities below any noble metal surface. As a proof, a circle having the theoretical diameter $D \sim 21$ Å [obtained from $D = 2Z_{imp}\tan(\beta/2)$] is shown in the left inset of Fig. 1A. In addition, we performed the identical procedure to determine the depths of the impurities observed in the STM measurements.

The strong directionality of electron propagation is not unique to copper and has many consequences for other materials. Once the shape of the propagator is known, either by STM investigation, calculations based on the band-structure, or quick estimates from a knowledge of the Fermi surface, many physical effects can be easily predicted. We have demonstrated and explained the very anisotropic CDO caused by subsurface point defects. Of course, similar behavior will be found for both spin channels if the impurity is magnetic, in the arrangement of the Kondo-screening cloud if the system is below the Kondo-temperature, and for the indirect exchange (RKKY)-interaction between two magnetic atoms (Fig. 4C).

By scrutinizing the real-space properties of the single-electron propagator and settling the explicit relation between the Fermi surface shape and the anisotropic charge oscillations, we demonstrate a new application of STM: visualization of Fermi surfaces in real space. The LDOS pattern as function of energy is determined by (i) the dispersion of host-metal band structure, (ii) the energy-dependent coherence length of the quasiparticles, and (iii) the energy-dependent scattering phase shift of the impurity. With the use of spectroscopic STM techniques, our approach can provide access to constant-energy surfaces apart from the Fermi surface. For energies close to E_F, effects due to decoherence can be neglected, and even for $|\varepsilon - E_F| = 1$ eV, the mean free path is much larger than the distances between impurity and surface (*19*, *20*). Thus, for magnetic impurities, for instance, the information in the focusing pattern is dominated by the scattering behavior of the impurity, and the focusing effect can be applied to investigate the electronic properties of subsurface impurities spectroscopically.

The beamlike propagation paths could, for example, be used to construct a "nano-sonar" (Fig. 4A). Such a device could determine not only the depth and reflectivity of buried interfaces but also the position and magnetism of the interface. Here, in addition to the LDOS-oscillations of Fig. 1 caused by processes of direct propagation between impurity and surface, larger concentric rings should appear that are produced by electrons propagating from the impurity toward the interface and being reflected toward the surface. In fact, we extracted CDO and spin-dependent CDO for an interface of Co with Cu(111) using DFT calculations. These results allowed us to determine the position as well as the magnetism of the interface (supporting online material).

In ferromagnets, the Fermi surfaces and, consequently, the electron propagators are obviously different for the two spin channels. This should allow the design of effective spin filters (Fig. 4B). A mixture of both spin species enters the ferromagnet at a pointlike source contact (S↑↓) from which spin up– and spin down–electrons propagate in different directions and are collected at different drain contacts $D_\uparrow$ and $D_\downarrow$. According to recent theoretical calculations (*21*), body-centered cubic europium may be a good candidate for such an application.

References and Notes

1. M. F. Crommie, C. P. Lutz, D. M. Eigler, *Science* **262**, 218 (1993).
2. C. R. Moon *et al.*, *Science* **319**, 782 (2008).
3. F. Meier, L. Zhou, J. Wiebe, R. Wiesendanger, *Science* **320**, 82 (2008).
4. M. A. Ruderman, C. Kittel, *Phys. Rev.* **96**, 99 (1954).
5. J. Friedel, *Nuovo Cim.* **7** (suppl. 2), 287 (1958).
6. P. Grünberg, R. Schreiber, Y. Pang, M. B. Brodsky, H. Sowers, *Phys. Rev. Lett.* **57**, 2442 (1986).
7. M. Schmid, W. Hebenstreit, P. Varga, S. Crampin, *Phys. Rev. Lett.* **76**, 2298 (1996).
8. P. T. Sprunger, L. Petersen, E. W. Plummer, E. Lægsgaard, F. Besenbacher, *Science* **275**, 1764 (1997).
9. N. Quaas, M. Wenderoth, A. Weismann, R. Ulbrich, K. Schönhammer, *Phys. Rev. B* **69**, 201103 (2004).
10. M. Rose, A. Borg, T. Mitsui, D. F. Ogletree, M. Salmeron, *J. Chem. Phys.* **115**, 10927 (2001).
11. D. Shoenberg, *Nature* **183**, 171 (1959).
12. Y. V. Sharvin, L. M. Fisher, *JETP Lett.* **1**, 152 (1965).
13. V. S. Tsoi, *JETP Lett.* **19**, 70 (1974).
14. J. Heil, M. Primke, K. U. Würz, P. Wyder, *Phys. Rev. Lett.* **74**, 146 (1995).
15. D. A. Papaconstantopoulos, *Handbook of the Band Structure of Elemental Solids* (Plenum, New York, 1986).
16. P. Bruno, C. Chappert, *Phys. Rev. Lett.* **67**, 1602 (1991).
17. The denominator is also directly proportional to the effective mass tensor $\sqrt{\frac{d^2E}{dK_x^2}\cdot\frac{d^2E}{dK_y^2}}^{-1}$ (here, K_x and K_y are orthogonal wave vector coordinates that are located in a tangent plane on the Fermi surface). If one or both principal curvatures are zero (i.e., if the surface is cylindrical or flat), this quantity diverges and the expression $\Delta LDOS(\boldsymbol{x},\varepsilon) \propto \frac{1}{|c|R^2}$ breaks down. The LDOS in certain distances R then follows a different decay law ~ R^{-1} and ~ R^0, respectively.
18. N. Papanikolaou, R. Zeller, P. H. Dederichs, *J. Phys. Condens. Matter* **14**, 2799 (2002).
19. E. Knoesel, A. Hotzel, M. Wolf, *Phys. Rev. B* **57**, 12812 (1998).
20. I. Campillo, A. Rubio, J. M. Pitarke, A. Goldmann, P. M. Echenique, *Phys. Rev. Lett.* **85**, 3241 (2000).
21. J. Kunes, R. Laskowski, *Phys. Rev. B* **70**, 174415 (2004).

22. This work was supported by the European Science Foundation EUROCORES Programme Self-Organized NanoStructures under contract N. ERAS-CT-2003-980409, the Deutsche Forschungsgemeinschaft Priority Programme SPP1153, and the Deutsche Forschungsgemeinschaft Collaborative Research Centre SFB602.

Supporting Online Material

www.sciencemag.org/cgi/content/full/323/5918/1190/DC1
Materials and Methods
SOM Text
Fig. S1
References

19 November 2008; accepted 27 January 2009
10.1126/science.1168738

Conductance of a Single Conjugated Polymer as a Continuous Function of Its Length

Leif Lafferentz,[1] Francisco Ample,[2] Hao Yu,[3] Stefan Hecht,[3] Christian Joachim,[2] Leonhard Grill[1]*

The development of electronic devices at the single-molecule scale requires detailed understanding of charge transport through individual molecular wires. To characterize the electrical conductance, it is necessary to vary the length of a single molecular wire, contacted to two electrodes, in a controlled way. Such studies usually determine the conductance of a certain molecular species with one specific length. We measure the conductance and mechanical characteristics of a single polyfluorene wire by pulling it up from a Au(111) surface with the tip of a scanning tunneling microscope, thus continuously changing its length up to more than 20 nanometers. The conductance curves show not only an exponential decay but also characteristic oscillations as one molecular unit after another is detached from the surface during stretching.

A key challenge in molecular electronics (*1*) is the detailed understanding of charge transport through a single molecular wire (*2*–*4*). One of the first conductance measurements of a metal–single molecule–metal junction used a scanning tunneling microscope (STM); the STM tip made electrical contact to a single C_{60} molecule adsorbed on a metal surface (*5*). This result was soon followed by break junction experiments (*6*–*8*), in which an ultrathin metallic wire junction is mechanically broken, providing a two-electrode junction where a

statistical number of molecules can be located and where conductance histograms are collected to reveal the average conductance of presumably single molecules in this molecular junction (*9*, *10*). These two techniques demonstrated that electrons can easily tunnel through a molecule with a low energy gap between the highest occupied molecular orbital (HOMO) and lowest unoccupied molecular orbital (LUMO). This approach can be used to provide statistical information about the conductance of single or very few molecules. However, they do not allow the conductance of a single and long molecular wire to be determined as the function of the distance between the two contacts on the same molecule. We present an experimental procedure to measure the conductance of a single and the same molecular wire with a well-defined and defect-free chemical structure as a function of the distance between the two contact points on the wire while precisely imaging the molecule's conformation before and after the measurement with submolecular resolution.

Recently, it was reported that a single molecule can be picked up from a solid surface with scanning probe techniques by approaching the scanning tip toward the surface and subsequently lifting up a single or several molecules when retracting the tip. This method was applied to molecules (*11*–*17*) by STM and to oligomers (*18*) or DNA strands (*19*) by atomic force microscopy (AFM), although the latter one is not capable of conductance measurements. With such a pulling manipulation, one end of a molecule is bound to the tip of an STM while maintaining surface adsorption at the other end. The pulling was mostly practiced at random on many molecules at the same time, with no characterization of molecular conformations in the junction before and after (*11*–*16*). A few studies compared the statistically obtained conductances of an oligomer series of different lengths up to 7 nm (*13*–*15*). However, in the controlled pulling experiment on a single perylene-tetracarboxylic-dianhydride (PTCDA) molecule, the length of the molecule in the junction was fixed to only 1 nm (*17*).

Our measurements require long π-conjugated oligomers adsorbed on a surface that cannot be deposited intact by conventional sublimation techniques under clean conditions because of their large molecular weight (*20*). To access long one-dimensional molecular chains, polyfluorene composed of conjugated fluorene repeat units was targeted by our recently developed in situ polymerization (*21*). For this purpose, we used dibromoterfluorene (DBTF) monomers, consisting of three fluorene units, carrying lateral methyl groups and a Br atom at each end (Fig. 1A). These terminal groups are dissociated from the terfluorene (TF) molecular core in the first activation step of our on-surface synthesis (*21*). At a surface temperature of 10 K (*22*), single DBTF molecules on a Au(111) surface appeared in constant-current STM as three intense lobes corresponding to the dimethyl groups (Fig. 1B). DBTF molecules adopt a zig-zag shape on the

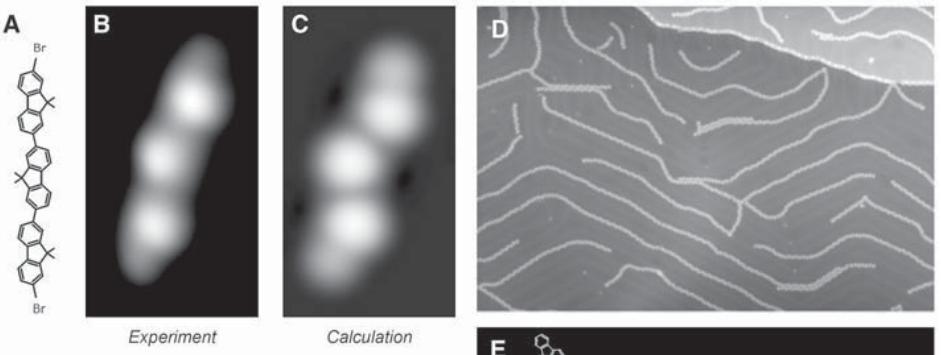

Fig. 1. On-surface polymerization of DBTF to conjugated molecular chains. (**A**) Chemical structure of DBTF molecules with experimental (**B**) and calculated (**C**) STM images (2.5 by 4.5 nm) of intact molecules, with bright protrusions associated with the lateral dimethyl groups. (**D**) Overview STM image (80 by 120 nm, 1 V, and 0.1 nA) after on-surface polymerization. The produced long covalently bound molecular chains, i.e., polyfluorene, follow the herringbone reconstruction of the substrate. (**E**) STM image (5.9 by 3.6 nm) of a single polyfluorene chain end with its chemical structure superimposed (using a different scaling). The arrows indicate three identical (in the STM image and the chemical structure), newly formed covalent bonds between individual building blocks.

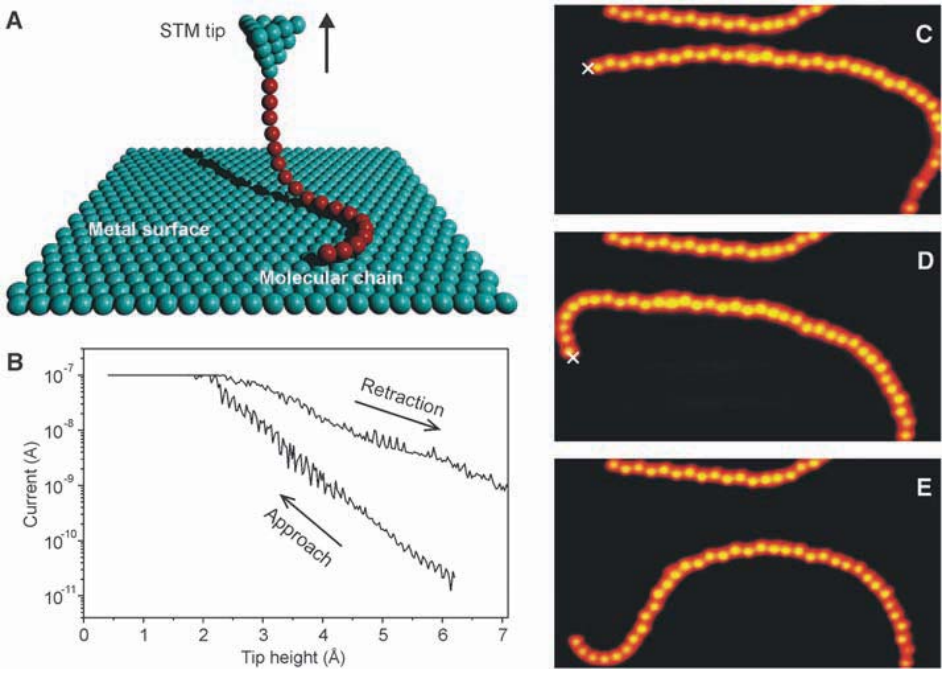

Fig. 2. Lifting a single molecular chain with the STM tip. (**A**) Scheme of the chain pulling procedure: After contacting a molecular chain to the STM tip, it can be lifted from the surface in a ropelike manner upon retraction because of its flexibility and weak interaction with the substrate. (**B**) Tunneling current as a function of the tip height during a vertical manipulation (approach and retraction with different slopes are marked by arrows). The maximum current is limited in this experiment to 100 nA (by the current preamplifier). (**C** to **E**) STM images (25.4 by 13.7 nm) of the same surface area during a vertical manipulation series (the cross indicates the position of tip approach and retraction). The manipulated chain, extending beyond the lower image border, changes its shape during the pulling processes. The fixed chain at the upper image border serves as reference.

[1]Physics Department, Freie Universität Berlin, 14195 Berlin, Germany. [2]Nanosciences Group, Centre d'Elaboration des Materiaux et d'Etudes Structurales (CEMES)–CNRS, 31055 Toulouse, France. [3]Department of Chemistry, Humboldt-Universität zu Berlin, 12489 Berlin, Germany.

*To whom correspondence should be addressed. E-mail: leonhard.grill@physik.fu-berlin.de

Au(111) surface, corresponding to the energetically favored alternate conformation of the methyl groups with respect to the molecular board (*22*). This result is in very good agreement with STM image calculations (Fig. 1C) that allow us to extract the exact position of each dimethyl group along a DBTF unit. Because of the low evaporator temperature during DBTF deposition, the Br atoms should still be attached to the TF core; a comparison between the observed and calculated images indicates that this is the case.

After heating the Au(111) surface up to 520 K for 5 min, the DBTF's Br atoms dissociate and covalent bonds are formed between different activated TF monomers, which diffuse randomly on the surface (Fig. 1D). The high mobility of the monomers, being a prerequisite for polymerization, is favored by the presence of lateral methyl groups on each monomer. Hence, this on-surface synthesis allows the formation of long, well-defined chains on the Au(111) surface; oligomer lengths greater than 100 nm were observed.

These polyfluorenes, carrying only methyl side groups, cannot be prepared by conventional polymerization processes in solution because of the absence of sufficiently solubilizing side chains. The homogeneous appearance of each molecular chain demonstrates the extreme regularity of their chemical composition, meaning that the newly formed covalent bonds are equivalent to the existing bonds, connecting the three fluorene units within each DBTF monomer, and that defect-free polymers were synthesized on the surface (Fig. 1E). The resulting polymers, commonly following the herringbone substrate reconstruction (Fig. 1D), are mobile enough on the Au(111) surface to be manipulated laterally with an STM tip for chains as long as 25 nm (*22*). Furthermore, the manipulation proves their high flexibility, enabling different curvatures of the chain without breaking the chemical bonds between the different TF monomers.

After selecting an isolated oligomer chain on the surface on the basis of a first STM image, this chain was pulled upward by the STM tip apex (Fig. 2A). For this purpose, the STM tip was first positioned at one end of the chain where, because of the Br dissociation during the on-surface synthesis, a chemical radical is presumably located. Subsequently, the tip apex was gently brought into close proximity of the selected chain to establish the electronic contact and then progressively retracted to lift it upward. The precise tip location on the molecular chain end is of great importance in this process, as evidenced by characteristic differences of the pulling success rate (*22*). The variation of the tunneling current I as a function of vertical distance z during this procedure was recorded, giving detailed insight into the vertical manipulation (Fig. 2B). After a characteristic $I(z)$ exponential increase during the tip approach to the surface (*23*), a different $I(z)$ dependence was recorded during retraction, when the molecular chain has been bonded to the tip apex. The current was much greater at the same value of z, when the tip is retracted very far from the surface, as compared to the case where no molecular chain was attached. Apparently, the tip-molecule interaction, which is less defined than the contact on the surface (that is imaged before the pulling experiment), is stronger than the chain segment's interaction with the substrate, keeping the chain attached to the tip during the pulling process. Although it is possible to lift entire chains from the surface, the tip-chain connection sometimes ruptures during the retraction (but not at constant tip-surface distance), which manifests as an abrupt drop of the tunneling current.

Complementary to the $I(z)$ curve, STM images recorded before and after a vertical manipulation can aid in the visualization of the changes in the chain conformation and position on the surface. The high mechanical stability of the STM junction (lateral and vertical drift of less than 7 pm/min) renders such a vertical STM manipulation extremely reliable for conductance measurements of long molecular wires. STM images before and after two vertical manipulations are shown in Fig. 2C and Fig. 2, D and E, respectively. In each experiment, the STM tip picked up a single chain and dropped it down (after an arbitrary retraction distance), as monitored by the $I(z)$ curve. The polymer in Fig. 2D is not imaged at the same position as before the pulling (Fig. 2C) but has moved to the left, following the pulled chain end in a ropelike manner. The consequence of the pulling-release sequence is that the initial linear conformation of the chain first adopts a left- and then a right-handed curvature with a large lateral displacement of the contacted chain end (Fig. 2D). Such a modification of the molecular conformation is hardly possible to obtain by lateral manipulation when the full chain remains adsorbed on the surface. Furthermore, we have not observed chain scission during any of the several hundreds of vertical manipulation procedures.

To measure the charge transport through a constructed surface–single molecule–tip junction as a function of the distance, the junction conductance variation $G(z)$ was recorded at a 100 mV bias voltage while pulling a given molecular chain (Fig. 3A). At low temperature, $G(z)$ reflects the ability of the chain to electronically couple the two electrodes of the STM junction through its more or less delocalized electronic structure as a function of the distance between the two electronic contact points on the chain (the surface and the tip apex) (*24*). Fitting $G(z)$ by the exponential

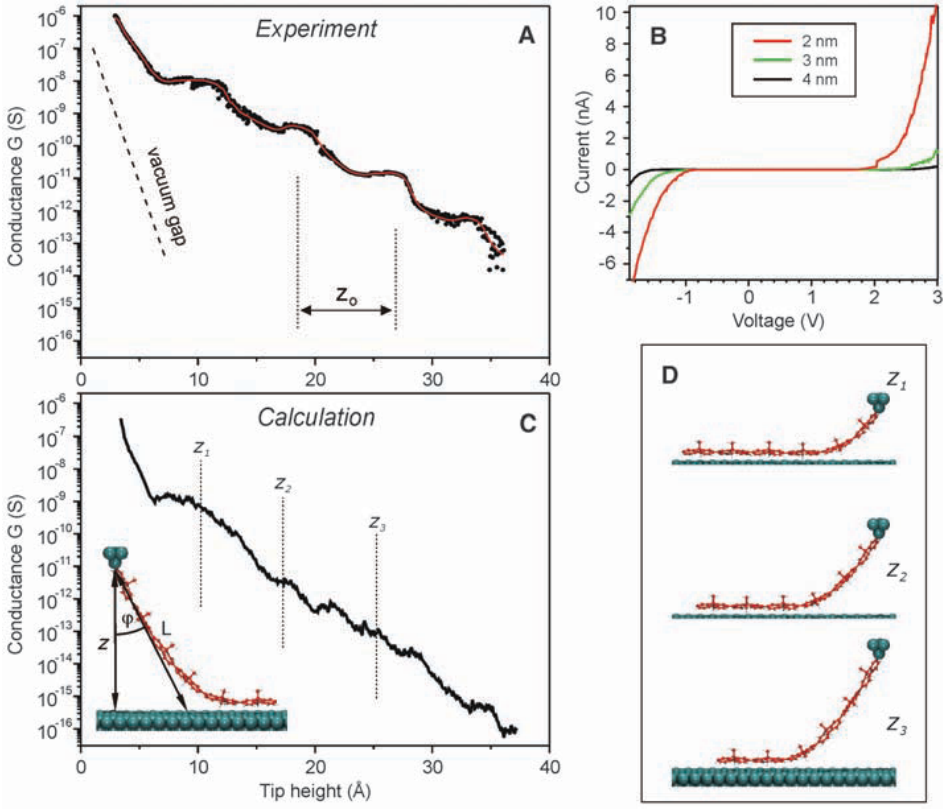

Fig. 3. Conductance as a function of the length of the molecular wire. Experimental (**A**) and calculated (**C**) $G(z)$ curves (equally scaled), both exhibiting characteristic oscillations with a period of z_o (the decay of a vacuum gap is plotted for comparison). The experimental curve is composed of two data sets from measurements below and above about 20 Å, respectively, using different setups and thus ranges for current detection (each about four orders of magnitude). (**B**) *I-V* curves (of single wires and thus not averaged) at three tip-surface distances (2, 3, and 4 nm). (**D**) Schematic views of characteristic conformations during the pulling process, just before the detachment of another molecular unit (z_1 = 10.2 Å, z_2 = 17.2 Å, and z_3 = 25.2 Å). The inset in (C) shows a sketch with the characteristic parameters z, L, and φ.

relationship $G = G_o \times e^{-\beta z}$ (*25*), a damping factor β of 0.38 ± 0.09 Å^{-1} is obtained experimentally. This value, a measure for the conductance of the molecular chain, is in very good agreement with the calculated one of 0.36 Å^{-1} [calculations were done with the Extended Hückel Molecular Orbital Theory–Elastic Scattering Quantum Chemistry (EHMO-ESQC) method (*22*)]. The average value of G_o, which is determined by the contacts to the electrodes, is 300 nS (with a variation between about 10 and 500 nS). The *z* distance is shorter than the real length of the molecular chain between the two contact points because of the ropelike bending of the chain. Correcting β by taking into account the relation between *z* and the effective molecular wire length *L*, between the tip apex and the part of the molecular wire remaining adsorbed flat on the surface (Fig. 3C, inset), leads to $z = L.\cos\varphi$, that is, β = 0.3 Å^{-1}. The decay factor β is much less than the 2.4 Å^{-1} inverse decay length through a vacuum gap (indicated by a dashed line in Fig. 3A) (*2*), confirming that the electrons are tunneling through a single molecular chain. Other examples of molecular wires with smaller β values have been reported. However, they also display smaller HOMO-LUMO gaps (*26*) than the polyfluorene molecular wire investigated here [a gap between 3 and 4 eV has been determined for similar poly(dioctylfluorene) molecules (*27*)].

With our pulling technique, the current through the wire can also be measured as a function of the bias voltage at any fixed wire length, that is, tip-sample distance, by stopping the pulling process. The characteristic asymmetric *I*(*V*) curves of such single molecular wires, taken, for instance, at *z* of 2, 3, and 4 nm in Fig. 3B, confirm the presence of two electronic resonance thresholds. We attribute these to the first reduced and oxidized states of the molecular wire, corresponding in a first approximation to its HOMO and LUMO levels, with the HOMO closer to the Fermi level than the LUMO, which leads to asymmetric *I*-*V* characteristics.

The exponential conductance decay of a molecular chain with increasing length should follow a linear curve on a logarithmic scale (*4*). However, the one presented in Fig. 3A is not straight but shows characteristic oscillations with maxima at retraction distances of 10, 19, 29, and 41 Å (with an error of about ±3 Å), that is, a typical oscillation period z_o of about 10 Å. Using the EHMO-ESQC calculation method (*22*), *G*(*z*) was calculated as presented in Fig. 3C, taking into account the mechanical deformation of the molecular wire, its sliding over the surface during the pulling process, and the full junction valence electronic structure, including the interaction with the tip apex and the physisorption of the molecular chain on the Au(111) surface at the other end, which defines the electronic contact of the molecular wire with the surface.

At small *z* values, a steep *G*(*z*) decay is observed both in the experimental and the calculated curve, due to the tunneling through vacuum at low tip heights. Aside from its general exponential trend at larger *z* values, the calculated *G*(*z*) (Fig. 3C) shows regular oscillations with a z_o between 6 and 8 Å, reproducing the experimental ones. Given the known optimized molecular chain conformation of a calculated pulling, we can attribute each oscillation maximum to a given monomer unit being adsorbed flat on the surface and about to be pulled away from the surface after a short sliding motion (see schemes in Fig. 3D). Hence, superimposed on the exponential decay trend, the contact conductance is oscillating because of the chainlike behavior that involves one monomer unit after the other being removed from contact with the surface by the pulling process. The maxima in the *G*(*z*) curve reflect the conformations slightly before the detachment of another chain unit (shown for three different heights in Fig. 3D) that in turn leads to an increased chain length between tip and surface and thus a drop of *G*(*z*). Interestingly, the electronic contact between one monomer of the chain and the surface is ensured by its π system and not by its methyl leg, which would cause a *G*(*z*) oscillation period of the order of the 2.88 Å Au(111) surface lattice constant (*22*). Instead, it must be of the order of the monomer unit length (8 to 9 Å), but not exactly equal to it because of the absent registry between the spatial extension of the monomer π system weakly overlapping with the surface and the Au(111) surface corrugation. The difference between the 10 Å experimental and our 7 Å calculated periods originates from the difficulty in theoretically reproducing in detail the full molecular mechanics of the total junction that arises from the large number of atoms involved. For example, upon pulling, the molecule is sliding but also snaking over the surface, a mechanical motion we have found difficult to reproduce in the calculation and which easily shifts the conductance oscillation by a few angstrom in the *z* direction.

Very often, the chain end to tip apex bond breaks before a complete vertical pulling, but in some cases, it remains attached to the tip until the entire chain is lifted up vertically. We measured the conductance of such extremely long molecular wires up to 20 nm in length. Figure 4A shows such a case, in which a single chain is lifted up at the left end (the position of the tip approach is marked by a cross). The *I*(*z*) curve during lifting (Fig. 4B) exhibits an abrupt decrease at the end of the pulling process and shows that the tip to surface electronic interaction through the molecular wire is lost exactly at a *z* = 20 nm distance. Hence, the chain is in a fully elongated conformation before the break, while being contacted vertically between the tip apex and the surface (Fig. 4C). To record the *I*(*z*) curve for large tip–molecular wire–surface junctions in Fig. 4B, it was necessary to increase the junction bias voltage continuously from –100 mV up to –4 eV during the pulling, compensating for the tunneling current exponential decay at low bias voltage. This result confirms that β is energy dependent, with a lower value in the energy gap

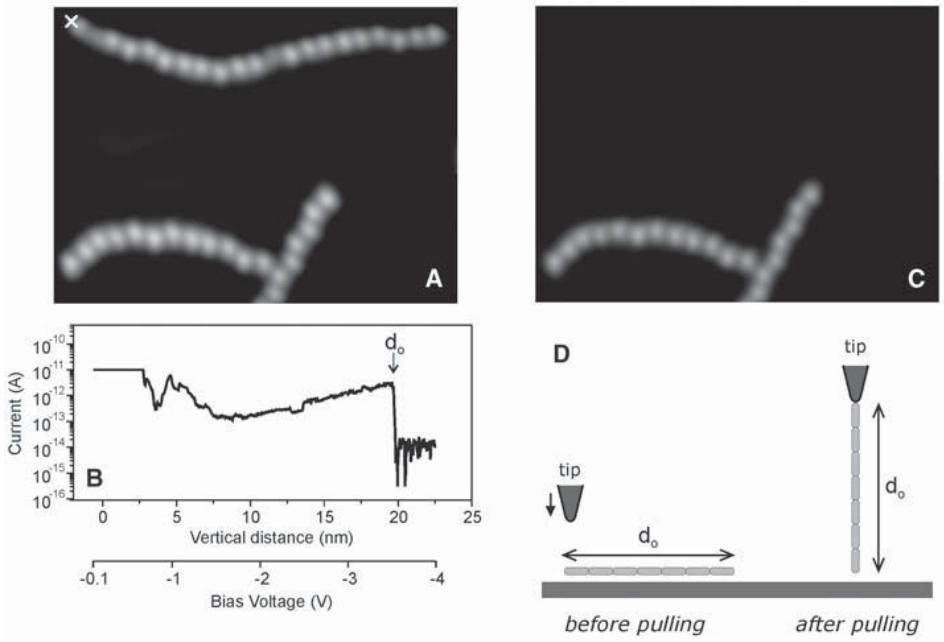

Fig. 4. Complete detachment of a long single chain. STM images (20 by 15 nm) before (**A**) and after (**C**) a vertical manipulation process in which the entire chain is lifted from the surface. (**B**) Current curve as a function of the vertical tip distance from the surface (the corresponding bias voltage scale is shown below). The abrupt decrease at a tip height of about 20 nm reflects the disruption of the tip-surface connection through the chain and hence its complete removal at a vertical distance equal to its length d_o. (**D**) Schematic views of the tip-chain configurations before and after this pulling process. At the end, the chain is attached vertically to the tip, which is thus elongated by d_o, and therefore removed from the surface [see (C)].

when approaching the HOMO or LUMO resonance of the molecular wire (*28*). The increased conductance at higher bias voltages then compensates for the molecular wire length increase in Fig. 4B (a factor of 40 is not sufficient for the achieved current increase). Thus, such a setup allows the determination of the small conductance (8.6×10^{-13} S) of a single and the same molecular wire with 20 nm length (the conductance at small bias voltages cannot be measured over such a large distance, due to the extremely low current—below the detection limit—passing through the polymer in this case). In this regard, it would be interesting to prepare and study conjugated polymers with smaller HOMO-LUMO gaps. Such molecular wires should exhibit higher conductances and allow charge transport to be determined over even larger distances.

References and Notes

1. C. Joachim, J. K. Gimzewski, A. Aviram, *Nature* **408**, 541 (2000).
2. A. Nitzan, *Annu. Rev. Phys. Chem.* **52**, 681 (2001).
3. A. Nitzan, M. A. Ratner, *Science* **300**, 1384 (2003).
4. N. J. Tao, *Nat. Nanotechnol.* **1**, 173 (2006).
5. C. Joachim, J. K. Gimzewski, R. R. Schlittler, C. Chavy, *Phys. Rev. Lett.* **74**, 2102 (1995).
6. M. A. Reed, C. Zhou, C. J. Muller, T. P. Burgin, J. M. Tour, *Science* **278**, 252 (1997).
7. R. M. H. Smit *et al.*, *Nature* **419**, 906 (2002).
8. J. Reichert *et al.*, *Phys. Rev. Lett.* **88**, 176804 (2002).
9. S. Wu *et al.*, *Nat. Nanotechnol.* **3**, 569 (2008).
10. M. Kiguchi *et al.*, *Phys. Rev. Lett.* **101**, 046801 (2008).
11. B. Xu, N. J. Tao, *Science* **301**, 1221 (2003).
12. W. Haiss *et al.*, *J. Am. Chem. Soc.* **125**, 15294 (2003).
13. X. Xiao, B. Xu, N. Tao, *J. Am. Chem. Soc.* **126**, 5370 (2004).
14. J. He *et al.*, *J. Am. Chem. Soc.* **127**, 1384 (2005).
15. S. H. Choi, B. Kim, C. D. Frisbie, *Science* **320**, 1482 (2008).
16. W. Haiss *et al.*, *Nat. Mater.* **5**, 995 (2006).
17. R. Temirov, A. Lassise, F. B. Anders, F. S. Tautz, *Nanotechnology* **19**, 065401 (2008).
18. F. Kühner, M. Erdmann, H. E. Gaub, *Phys. Rev. Lett.* **97**, 218301 (2006).
19. S. K. Kufer, E. M. Puchner, H. Gumpp, T. Liedl, H. E. Gaub, *Science* **319**, 594 (2008).
20. T. Zambelli *et al.*, *Int. J. Nanoscience* **3**, 331 (2004).
21. L. Grill *et al.*, *Nat. Nanotechnol.* **2**, 687 (2007).
22. Materials and methods are available as supporting material on *Science* Online.
23. L. Limot, J. Kröger, R. Berndt, A. Garcia-Lekue, W. A. Hofer, *Phys. Rev. Lett.* **94**, 126102 (2005).
24. C. Joachim, M. A. Ratner, *Proc. Natl. Acad. Sci. U.S.A.* **102**, 8801 (2005).
25. M. Magoga, C. Joachim, *Phys. Rev. B* **56**, 4722 (1997).
26. M. Magoga, C. Joachim, *Phys. Rev. B* **57**, 1820 (1998).
27. D. Neher, *Macromol. Rapid Commun.* **22**, 1365 (2001).
28. C. Joachim, M. Magoga, *Chem. Phys.* **281**, 347 (2002).

29. Financial support from the European Integrated Project PICO INSIDE and the Deutsche Forschungsgemeinschaft (DFG) through SFB 658 and contract GR 2697/1-2 is gratefully acknowledged.

Supporting Online Material

www.sciencemag.org/cgi/content/full/323/5918/1193/DC1
Materials and Methods
Figs. S1 to S6
References

10 November 2008; accepted 16 January 2009
10.1126/science.1168255

Early Hominin Foot Morphology Based on 1.5-Million-Year-Old Footprints from Ileret, Kenya

Matthew R. Bennett,[1]* John W.K. Harris,[2] Brian G. Richmond,[3,4] David R. Braun,[5] Emma Mbua,[6] Purity Kiura,[6] Daniel Olago,[7] Mzalendo Kibunjia,[6] Christine Omuombo,[7] Anna K. Behrensmeyer,[8] David Huddart,[9] Silvia Gonzalez[9]

Hominin footprints offer evidence about gait and foot shape, but their scarcity, combined with an inadequate hominin fossil record, hampers research on the evolution of the human gait. Here, we report hominin footprints in two sedimentary layers dated at 1.51 to 1.53 million years ago (Ma) at Ileret, Kenya, providing the oldest evidence of an essentially modern human–like foot anatomy, with a relatively adducted hallux, medial longitudinal arch, and medial weight transfer before push-off. The size of the Ileret footprints is consistent with stature and body mass estimates for *Homo ergaster/erectus*, and these prints are also morphologically distinct from the 3.75-million-year-old footprints at Laetoli, Tanzania. The Ileret prints show that by 1.5 Ma, hominins had evolved an essentially modern human foot function and style of bipedal locomotion.

Bipedalism is a key human adaptation that appears in the fossil record by 6 million years ago (Ma) (*1*). Considerable debate continues over when and in what context a modern human–like form of bipedalism evolved, because of a fragmentary record and disagreements over the functional interpretations of existing fossils and footprints (*2*–*7*). Modern human footprints reflect the specialized anatomy and function of the human foot, which is characterized by a fully adducted hallux, a large and robust calcaneus and tarsal region, a pronounced medial longitudinal arch, and short toes (*2*). Footprints reflect the pressure distribution as the foot makes contact with the substrate, but also the sediment's geomechanical properties (*8*). During normal walking, the weight-bearing foot undergoes a highly stereotypical movement and pressure distribution pattern in which the heel contacts the ground first, making a relatively deep impression on the substrate. This is followed by contact with the lateral side of the foot and metatarsal heads, after which weight transfers to the ball of the foot with peak pressure under the medial metatarsal heads, and finally ending with toe-off pressure under the hallux (*9*, *10*). As a consequence, the deepest part of a footprint often occurs beneath the first and second metatarsal heads, that along with a deep hallucal impression corresponds to the peak pressures at toe-off (*10*). The extent to which any pressure, or footprint impression, occurs medially varies with the anatomy of the midfoot, including the height of the longitudinal arch and other factors (*11*), and the extent to which lateral toes leave impressions depends on factors such as foot orientation relative to the direction of travel, transverse versus oblique push-off axes, and substrate properties. This contrasts with the less stereotypical pattern of footfall observed in African apes during quadrupedal and bipedal locomotion. Here the heel and lateral mid-foot make contact with the ground first, followed by contact with the lateral toes that are often curled and with a hallux that is often widely abducted. Lift-off in the African apes is variable, but it usually involves relatively low pressure during final contact by both the lateral toes and widely abducted hallux, in stark contrast to modern human foot function (*11*).

Here, we report hominin footprints from the Okote Member of the Koobi Fora Formation (*12*), second in age only to the mid-Pliocene (3.7 Ma) Laetoli prints (*13*), located close to Ileret, Kenya (Fig. 1; site FwJj14E; latitude 4°18′44″N, longitude 36°16′16″E). The footprints are found in association with animal prints on two stratigraphically separated levels and were digitized with an optical laser scanner (Fig. 1) (*14*). The upper surface contains three hominin footprint trails comprising two trails of two prints and one of seven prints, as well as a number of isolated prints (Figs. 2 and 3 and figs. S3 and S6 to S11). The lower surface, approximately 5 m below, preserves one trail of two prints and a single isolated hominin print (Fig. 3). The footprints occur within a 9-m-thick sequence of fine-grained, normally

[1]School of Conservation Sciences, Bournemouth University, Poole, BH12 5BB, UK. [2]Department of Anthropology, Rutgers University, 131 George Street, New Brunswick, NJ 08901, USA. [3]Center for the Advanced Study of Hominid Paleobiology, Department of Anthropology, George Washington University, Washington, DC 20052, USA. [4]Human Origins Program, National Museum of Natural History, Smithsonian Institution, Washington, DC 20013–7012, USA. [5]Department of Archaeology, University of Cape Town, Private Bag, Rondebosch 7701, South Africa. [6]National Museums of Kenya, Post Office Box 40658-00100, Nairobi, Kenya. [7]Department of Geology, University of Nairobi, Post Office Box 30197, Nairobi, Kenya. [8]Department of Paleobiology, MRC 121, National Museum of Natural History, Smithsonian Institution, Washington, DC, 20013–7012, USA. [9]School of Biological and Earth Sciences, Liverpool John Moores University, Liverpool, L3 3AF, UK

*To whom correspondence should be addressed. E-mail: mbennett@bmth.ac.uk